The evolutionary dynamics of influenza A virus within and between human hosts

Running Title: Influenza dynamics within and between hosts

John T. McCrone[1], Robert J. Woods[2], Emily T. Martin[3], Ryan E. Malosh[3], Arnold S. Monto[3], and Adam S. Lauring[1,2 *]

[1] Department of Microbiology and Immunology, University of Michigan, Ann Arbor, MI 48109

[2] Division of Infectious Diseases, Department of Internal Medicine, University of Michigan, Ann Arbor, MI 48109

[3] Department of Epidemiology, University of Michigan, Ann Arbor, MI 48109

* Corresponding author

Adam S. Lauring

1150 W. Medical Center Dr.

MSRB1 Room 5510B

Ann Arbor, MI 48109-5680

(734) 764-7731

alauring@med.umich.edu

Abstract Word Count:

Main Text Word Count:

Key Words – influenza virus, bottleneck, transmission, diversity, evolution

Abstract

A complete understanding of influenza virus evolution requires studies at all levels, as viral evolutionary dynamics may differ across spatial and temporal scales. The relative contribution of deterministic processes, such as selection, and stochastic processes, such as genetic drift, is influenced by the virus' effective population size. While the global evolution of influenza A virus (IAV) is dominated by the positive selection of novel antigenic variants that circulate in the tropics, much less is known about the virus' evolution within and between human hosts. With few exceptions, most of the available data derive from studies of chronically infected, immunocompromised hosts, experimental infections with attenuated viruses, or animal models. Here we define the evolutionary dynamics of IAV in human hosts through next generation sequencing of 249 upper respiratory specimens from 200 individuals collected over 6290 person-seasons of observation. Because these viruses were collected over 5 seasons from individuals in a prospective community-based cohort, they are broadly representative of natural human infections with seasonal viruses. Within host genetic diversity was low, and we found little evidence for positive selection of minority variants. We used viral sequence data from 35 serially sampled individuals to estimate a within host effective population size of 30-50. This estimate is consistent across several models and robust to the models' underlying assumptions. We also identified 43 epidemiologically linked and genetically validated transmission pairs. Maximum likelihood optimization of multiple transmission models estimates an effective transmission bottleneck of 1-2 distinct genomes. Our data suggest that positive selection of novel viral variants is inefficient at the level of the individual host and that genetic drift and other stochastic processes dominate the within and between host evolution of influenza A viruses.

Introduction

The rapid evolution of influenza viruses has led to reduced vaccine efficacy, widespread drug resistance, and the continuing emergence of novel strains. Broadly speaking, evolution is the

product of deterministic processes, such as selection, and stochastic processes, such as genetic drift (1). The relative contribution of each is greatly affected by the effective population size, or size of an idealized population whose dynamics are similar to that of the population in question (2). If the effective population size of a virus is large, as in quasispecies models, evolution is largely deterministic and the frequency of a mutation can be predicted based on its starting frequency and selection coefficient. In small populations, selection is inefficient, and changes in mutation frequency are strongly influenced by genetic drift.

Viral dynamics may differ across spatial and temporal scales, and a complete understanding of influenza evolution requires studies at all levels (3, 4) .The global evolution of influenza A virus (IAV) is dominated by the positive selection of novel antigenic variants that circulate in the tropics and subsequently seed annual epidemics in the Northern and Southern hemisphere (5). Whole genome sequencing has also demonstrated the importance of intrasubtype reassortment to the emergence of diverse strains that differ in their antigenicity. While continual positive selection of antigenically drifted variants drives global patterns, whole genome sequencing of viruses on more local scales suggests the importance of stochastic processes such as strain migration and within-clade reassortment (6).

With the advent of next generation sequencing, it is now feasible to efficiently sequence patient-derived isolates at sufficient depth of coverage to define the diversity and dynamics of virus evolution within individual hosts (7). Studies of IAV populations in animal and human systems suggest that most intrahost single nucleotide variants (iSNV) are rare and that intrahost populations are subject to strong purifying selection (8-14). While positive selection of adaptive variants is commonly observed in cell culture (15-17), it has only been documented within human hosts in the extreme cases of drug resistance (8, 18, 19), long-term infection of immunocompromised hosts (20) or experimental infections with attenuated viruses (21). Indeed,

53 we and others have been unable to identify evidence for positive selection in natural human
54 infections (13, 14), and its relevance to within host processes is unclear.
55
56 Despite limited evidence for positive selection, it is clear that novel mutations do arise within
57 hosts. Their potential for subsequent spread through host populations is determined by the size
58 of the transmission bottleneck (22, 23). If the transmission bottleneck is sufficiently wide, low
59 frequency variants can plausibly be transmitted and spread through host populations (24).
60 Because the transmission bottleneck is conceptually similar to the effective population size
61 between hosts, its size will also inform the relative importance of selection and genetic drift in
62 determining which variants are transmitted. While experimental infections of guinea pigs and
63 ferrets suggest a very narrow transmission bottleneck (25, 26), studies of equine influenza
64 support a bottleneck wide enough to allow transmission of rare iSNV (9, 27). The only available
65 genetic study of influenza virus transmission in humans estimated a remarkably large
66 transmission bottleneck, allowing for transmission of 100-200 genomes (11, 28).
67
68 Here, we use next generation sequencing of within host influenza virus populations to define the
69 evolutionary dynamics of influenza A viruses (IAV) within and between human hosts. We apply
70 a benchmarked analysis pipeline to identify iSNV and to characterize the genetic diversity of
71 H3N2 and H1N1 populations collected over five post-pandemic seasons from individuals
72 enrolled in a prospective household study of influenza. We use these data to estimate the *in*
73 *vivo* mutation rate and the within and between host effective population size. We find that
74 intrahost populations are characterized by purifying selection, a small effective population size,
75 and limited positive selection. Contrary to what has been previously reported for human
76 influenza transmission (11), but consistent with what has been observed in other viruses (23),
77 we identify a very tight transmission bottleneck that limits the transmission of rare variants.
78

Results

We used next generation sequencing to characterize influenza virus populations collected from individuals enrolled in the Household Influenza Vaccine Effectiveness (HIVE) study (29-32), a community-based cohort that enrolls 213-340 households of 3 or more individuals in Southeastern Michigan each year (Table 1). These households are followed prospectively from October to April, with symptom-triggered collection of nasal and throat swab specimens for identification of respiratory viruses by RT-PCR (see Methods). In contrast to case-ascertained studies, which identify households based on an index case who seeks medical care, the HIVE study identifies individuals regardless of illness severity. In the first four seasons of the study (2010-2011 through 2013-2014), respiratory specimens were collected 0-7 days after illness onset. Beginning in the 2014-2015 season, each individual provided two samples, a self-collected specimen at the time of symptom onset and a clinic-collected specimen obtained 0-7 days later. Each year, 59-69% of individuals had self-reported or confirmed receipt of that season's vaccine prior to local circulation of influenza virus.

Over five seasons and nearly 6,290 person-seasons of observation, we identified 77 cases of influenza A/H1N1pdm09 infection and 313 cases of influenza A/H3N2 infection (Table 1). Approximately half of the cases (n=166) were identified in the 2014-2015 season, in which there was an antigenic mismatch between the vaccine and circulating strains (33). All other seasons were antigenically matched. Individuals within a household were considered an epidemiologically linked transmission pair if they were both positive for the same subtype of influenza virus within 7 days of each other. Several households had 3 or 4 symptomatic cases within this one-week window, suggestive of possible transmission chains (Table 1).

Within host populations have low genetic diversity

We processed all specimens for viral load quantification and next generation sequencing. Viral load measurements (genome copies per µl) were used for quality control in variant calling, which we have shown is highly sensitive to input titer (34) (Figure 1A). Accordingly, we report data on 249 high quality specimens from 200 individuals, which had a viral load of $>10^3$ copies per microliter of transport media, adequate RT-PCR amplification of all eight genomic segments, and an average read coverage of $>10^3$ across the genome (Table 1, Supplemental Figure 1).

We identified intrahost single nucleotide variants (iSNV) using our empirically validated analysis pipeline (34). Our approach relies heavily on the variant caller DeepSNV, which uses a clonal plasmid control to distinguish between true iSNV and errors introduced during sample preparation and/or sequencing (35). Given the diversity of influenza viruses that circulate locally each season, there were a number of instances in which our patient-derived samples had mutations that were essentially fixed (>0.95 frequency) relative to the clonal control. DeepSNV is unable to estimate an error rate for the control or reference base at these positions. We therefore performed an additional benchmarking experiment to identify a threshold for majority iSNV at which we could correctly infer whether or not the corresponding minor allele was also present (see Methods). We found that we could correctly identify a minor allele at a frequency of ≥2% when the frequency of the major allele was ≤98%. We therefore report data on iSNV present at frequencies between 2 and 98%. As expected, this threshold improved the specificity of our iSNV identification and decreased our sensitivity to detect variants below 5% compared to our initial validation experiment (34), which did not employ a frequency threshold (Supplemental Table 1).

Consistent with our previous studies and those of others, we found that the within host diversity of human influenza A virus (IAV) populations is low (11, 13, 14, 21, 34). Two hundred forty-three out of the 249 samples had fewer than 10 minority iSNV (median 2, IQR 1-3). There were 6

samples with greater than 10 minority iSNV. In 3 of these cases, the frequency of iSNVs were tightly distributed about a mean suggesting that the iSNV were linked and that the samples represented mixed infections. Consistent with this hypothesis, putative genomic haplotypes based on these minority iSNV clustered with distinct isolates on phylogenetic trees (Supplemental Figures 2 and 3). While viral shedding was well correlated with days post symptom onset (Figure 1A) the number of minority iSNV identified was not affected by the day of infection, viral load, subtype, or vaccination status (Figure 1B and Supplemental Figure 4).

The vast majority of minority variants were rare (frequency 0.02-0.07), and iSNV were distributed evenly across the genome (Figure 1C and 1D). The ratio of nonsynonymous to synonymous variants was 0.64 and was never greater than 1 in any 5% bin, which suggests that within host populations were under purifying selection. We also found that minority variants were rarely shared among multiple individuals. Ninety-five percent of minority iSNV were only found once, 4.7% were found in 2 individuals, and no minority iSNV were found in more than 3 individuals. The low level of shared diversity suggests that within host populations were exploring distinct regions of sequence space with little evidence for parallel evolution. Of the 31 minority iSNV that were found in multiple individuals (triangles in Figure 1D), 4 were nonsynonymous.

Although the full range of the H3 antigenic sites have not been functionally defined, it is estimated that 131 of the 329 amino acids in HA1 lie in or near these sites (36). We identified 17 minority nonsynonymous iSNV in these regions (Supplemental Table 2). Six of these were in positions that differ among antigenically drifted viruses (37, 38), and two (193S and 189N) lie in the “antigenic ridge” that is a major contributor to drift (39). Three of these have been detected at the global level as consensus variants since the time of isolation (128A, 193S and 262N) with two (193S and 262N) seemingly increasing in global frequency (40) (Supplemental Figure 5).

Additionally, we identified 1 putative H1N1 antigenic variant (208K in C_a) (41, 42). In total, putative antigenic variants account for 1.0-2.5% of minority iSNV identified and were found in 3.5-7.5% of infections. None of these iSNV were shared among multiple individuals.

Estimation of effective population size

Given the above observations, we hypothesized that within host populations of IAV are under purifying selection and that variants that rise to detectable levels do so by a neutral process as opposed to positive selection. Consistent with this hypothesis, we found that nonsynonymous and synonymous iSNV exhibited similar changes in frequency over time in the 35 individuals who provided serial specimens that contained iSNV (Figure 2A and 2B). We used the diffusion approximation to the Wright-Fisher model in conjunction with maximum likelihood estimation to determine the within host effective population size (N_e) of IAV (43). This model assumes that changes in iSNV frequency are due solely to random genetic drift and not selection, that iSNV are independent of one another, and that the effective population is sufficiently large to justify a continuous approximation to changes in allele frequency. While it is impossible to predict with certainty the trajectory of allele frequencies under random genetic drift, the Wright-Fisher model, and the diffusion approximation in particular, assigns probabilities to frequency changes given an N_e and the number of generations between sample times. In our model we fixed the within host generation time as either 6 or 12 hours (24) and report the findings for the 6 hour generation time below. We then asked what population size makes the observed changes in frequency most likely (Figure 2B). We restricted this analysis to samples taken at least 1 day apart (n = 29), as there was very little change in iSNV frequency in populations sampled twice on the same day (R = 0.990, Figure 2B and Supplemental Figure 6). The concordance of same day samples suggests that our sampling procedure is reproducible and that less than a generation had passed between samplings. Maximum likelihood optimization of this diffusion model revealed a within host effective population size of 35 (95% CI 26-46, Table 2).

The diffusion approximation makes several simplifying assumptions, which if violated could influence our findings. In particular, the model assumes a large population. To ensure our results were robust to this assumption, we employed a discrete interpretation of the Wright-Fisher model which makes no assumptions about population size (44). In this case we found an effective population size of 32 (95% CI 28-41), very close to our original estimate (Table 2). Both models assume complete independence of iSNV. To ensure this assumption did not affect our results, we fit the discrete model 1000 times, each time randomly subsetting our data such that only one iSNV per individual was included. This simulates a situation in which all modeled iSNV are independent and our assumption is met. Under these conditions we found a median effective population size of 33 (IQR 32-40), demonstrating negligible bias in the initial analysis due to correlation between iSNV.

As above, most iSNV in the longitudinal samples were rare (< 10%) and many became extinct between samplings. To ensure that our models were capable of accurately estimating the effective population size from such data, we simulated 1000 Wright-Fisher populations with iSNV present at approximately the same starting frequencies as in our data set an N_e of 30, 50, or 100. In these simulations, we found mean N_e of 34, 56 and 117 (Figure 2C), which suggests that our estimate is not an artifact of the underlying data structure.

To this point, we have assumed that neutral processes are responsible for the observed changes in iSNV frequency within hosts. Although this assumption seems justified at least in part by the analysis above, we tested the robustness of our models by fitting the nonsynonymous (n = 27) and synonymous iSNV (n = 36) separately. Here, we estimated an effective population size of 30 using the nonsynonymous iSNV and an effective population size of 37 using the synonymous iSNV (Table 2). These estimates are very close to that derived

from the whole dataset and suggest that nonsynonymous and synonymous mutations are influenced by similar within host processes. To further ensure that our results were not driven by a few outliers subject to strong selection, we ranked iSNV by their change in frequency over time and consecutively removed iSNV with the most extreme changes. We estimated the effective population size at each iteration and found we would have to remove the top 75% most extreme iSNV to increase the effective population size by a factor of 10 (Figure 2D). Therefore, our estimates are robust to a reasonable number of non-neutral sites. Finally, we also applied a separate Approximate Bayesian Computational (ABC) method, which uses a non-biased moment estimator in conjunction with ABC to estimate the effective population size of a population as well as selection coefficients for the iSNV present (17, 45). This distinct approach relaxes our assumption regarding neutrality. We applied this analysis to the 16 longitudinal pairs that were sampled 1 day apart and estimated an effective population of 54. We were unable to reject neutrality for just 4 of the 35 iSNV in this data set (Figure 2E). These four mutations were distributed between 2 individuals. Each individual had one nonsynonymous iSNV and one synonymous iSNV. Neither were putative antigenic variants.

Identification of forty-three transmission pairs

The amount of diversity that passes between individuals during transmission determines the extent to which within host evolution can affect larger evolutionary trends. We analyzed virus populations from 85 households with concurrent infections to quantify the level of shared viral diversity and to estimate the size of the IAV transmission bottleneck (Table 1). Because epidemiological linkage does not guarantee that concurrent cases constitute a transmission pair (46), we used a stringent rubric to eliminate individuals in a household with co-incident community acquisition of distinct viruses. We considered all individuals in a household with symptom onset within a 7-day window to be epidemiologically linked. The donor in each putative pair was defined as the individual with the earlier onset of symptoms. We discarded a

transmission event if there were multiple possible donors with the same day of symptom onset. Donor and recipients were not allowed to have symptom onset on the same day, unless the individuals were both index cases for the household. In these 6 instances, we analyzed the data for both possible donor-recipient directionalities. Based on these criteria, our cohort had 124 putative household transmission events over 5 seasons (Table 1). Of these, 52 pairs had samples of sufficient quality for reliable identification of iSNV from both individuals.

We next used sequence data to determine which of these 52 epidemiologically linked pairs represented true household transmission events as opposed to coincident community-acquired infections. We measured the genetic distance between influenza populations from each household pair by L1-norm and compared these distances to those of randomly assigned community pairs within each season (Figure 3A, see also trees in Supplemental Figures 2 and 3). While the L1-norm of a pair captures differences between the populations at all levels, in our cohort, it was largely driven by differences at the consensus level. We only considered individuals to be a true transmission pair if they had a genetic distance below the 5th percentile of the community distribution of randomly assigned pairs (Figure 3A). Forty-seven household transmission events met this criterion (Figure 3B). Among these 47 sequence-validated transmission pairs, 3 had no iSNV in the donor and 1 additional donor appeared to have a mixed infection. These four transmission events were removed from our bottleneck analysis as donors without iSNV are uninformative and mixed infections violate model assumptions of site independence (see Methods). We estimated the transmission bottleneck in the remaining 43 high-quality pairs (37 H3N2, 6 H1N1, Figure 3B).

A transmission bottleneck restricts the amount of genetic diversity that is shared by both members of a pair. We found that few minority iSNV where polymorphic in both the donor and recipient populations (Figure 3C). Minority iSNV in the donor were either absent or fixed in the

recipient (top and bottom of plot). The lack of shared polymorphic sites (which would lie in the middle of the plot in Figure 3C) suggests a stringent effective bottleneck in which only one allele is passed from donor to recipient.

Estimation of the transmission bottleneck

We applied a simple presence-absence model to quantify the effective transmission bottleneck in our cohort. True to its name, the presence-absence model simply measures whether or not a donor allele is present or absent in the recipient sample. Under this model, transmission is a neutral, random sampling process, and the probability of transmission is simply the probability that the iSNV will be included at least once in the sample given its frequency in the donor and the sample size, or bottleneck. We estimated a distinct bottleneck for each transmission pair and assumed these bottlenecks followed a zero-truncated Poisson distribution. This model also assumes that the sensitivity for detection of transmitted iSNVs is perfect and that each genomic site is independent of all others. We then used maximum likelihood optimization to determine the distribution of bottleneck sizes that best fit the data. We found a zero-truncated Poisson distribution with a mean of 1.66 (lambda = 1.12; 0.51-1.99, 95% CI) best described the data. This distribution indicates that the majority of bottlenecks are 1, and that very few are greater than 5 (probability 0.2%). There were no apparent differences between H3N2 and H1N1 pairs. The model fit was evaluated by simulating each transmission event 1,000 times. The presence or absence of each iSNV in the recipient was noted and the probability of transmission given donor frequency determined. The range of simulated outcomes matched the data well, which suggests that transmission is a selectively neutral event characterized by a stringent bottleneck (Figure 3D).

The majority of transmitted iSNV were fixed in the recipients. Although this trend matches the expectation given a small bottleneck, these data could also be consistent with a model in which

the probability of transmission is determined by the frequency at which iSNV are found at the community level. To ensure our bottleneck estimates were an outcome of neutral transmission and not an artifact of the larger community population structure or selection for the community consensus, we created a null model by randomly assigning community "recipients" to each donor in our transmission pairings. Each community "recipient" was drawn from the pool of individuals that were infected after the donor but in the same season and with the same subtype as the donor. We then identified whether or not each donor iSNV was found in the community recipient and determined the relationship between donor frequency and probability of "transmission" for 1,000 such simulations. Given the low level of diversity in our cohort, we predicted that rare iSNV would be unlikely to be found in a random sample, while the major alleles should be fixed in most random samples. This trend is clearly demonstrated in Figure 3E. It is also clear that this null model fit the data much more poorly than the presence/absence model, suggesting that the observed data in our bona fide transmission pairs were not a product of community metapopulation structure, but rather an outcome of neutral sampling events.

Because our bottleneck estimates were much lower than what has previously been reported for human influenza (11), we investigated the impact that our simplifying assumptions could have on our results. In particular, the presence-absence model assumes perfect detection of variants in donor and recipient, and it can therefore underestimate the size of a bottleneck in the setting of donor-derived variants that are transmitted but not detected in the recipient. These "false negative" variants can occur when the frequency of an iSNV drifts below the level of detection (e.g. 2% frequency) or when the sensitivity of sequencing is less than perfect for variants at that threshold (e.g. 15% sensitivity for variants at a frequency 2-5%). Leonard *et al.* recently suggested that a beta binomial transmission model can account for the stochastic loss of transmitted variants, by allowing for a limited amount of time-independent genetic drift within the recipient (28). We modified this model to also account for our benchmarked sensitivity for rare

variants (Supplemental Table 1). For all donor-derived iSNV that were absent in the recipient, we estimated the likelihood that these variants were transmitted but either drifted below our level of detection or drifted below 10% and were missed by our variant identification. Despite the relaxed assumptions provided by this modified beta binomial model, maximum likelihood estimation only marginally increased the average bottleneck size (mean 1.71: lambda 1.19; 0.55-2.12, 95%CI) relative to the simpler presence-absence model. We simulated transmission and subsequent random drift using the beta binomial model and the estimated bottleneck distribution as above (Figure 3F). Although the model matched the data well, the fit was not substantially better than that of the presence-absence model (AIC 75.5 for beta-binomial compared to 76.7 for the presence-absence model).

The mutation rate of influenza A virus within human hosts

The stringent influenza transmission bottleneck suggests that most infections are founded by one lineage and develop under essentially clonal processes. The diffusion approximation to the Wright-Fisher model (see above and Figure 2) can be used to predict the rate at which homogenous populations diversify from a clonal ancestor as a function of mutation rate and effective population size (2). By applying maximum likelihood optimization to the model and the frequency distribution of observed alleles (Figure 1C) we estimated an *in vivo* neutral mutation rate of 4×10^{-6} mutations per nucleotide per replication cycle and a within host effective population size of 33 (given a generation time of 6 hours). This is consistent with the estimates above. As we have recently estimated that 13% of mutations in influenza A virus are neutral (47), we estimated that the true *in vivo* mutation rate would be approximately 8 fold higher than our neutral rate – on the order of $3\text{-}4 \times 10^{-5}$. This in vivo mutation rate is close to our recently published estimate of influenza A mutation rates in epithelial cells by fluctuation test (48).

Discussion

We find that seasonal influenza A viruses replicate within and spread among human hosts with very small effective population sizes. Because we used viruses collected over five influenza seasons from individuals enrolled in a prospective household cohort, these dynamics are likely to be broadly representative of many seasonal influenza infections. Other notable strengths of our study include a validated sequence analysis pipeline and the use of models that are robust to the underlying assumptions. The small effective size of intrahost populations and the tight transmission bottleneck suggest that stochastic processes, such as genetic drift, dominate influenza virus evolution at the level of individual hosts. This stands in contrast to prominent role of positive selection in the global evolution of seasonal influenza.

While influenza virus populations are subject to continuous natural selection, selection is an inefficient driver of evolution in small populations (2). Despite a large census, our findings indicate that intrahost populations of influenza virus behave like much smaller populations. We therefore expect random drift to be the major force driving the evolution of influenza virus within human hosts. This finding contradicts previous studies, which have found signatures of adaptive evolution in infected hosts (8, 19, 21, 49). However, these studies rely on data from infections in which selective pressures are likely to be particularly strong (e.g. due to drug treatment or infection with a poorly adapted virus), or in which the virus has been allowed to propagate for extended periods of time. Under these conditions, one can identify the action of positive selection on within host populations. We suggest that these are important exceptions to the drift regime defined here.

We used both a simple presence-absence model and a more complex beta binomial model to estimate an extremely tight transmission bottleneck. The small bottleneck size is driven by the fact that within host diversity was low, and there were very few minority iSNV shared among individuals in a transmission chain. While our methods for variant calling may be more

364 conservative than those used in similar studies, it is unlikely that our small bottleneck is an
365 artifact of this stringency. The beta binomial model accounts for false negative iSNV (i.e.
366 variants that are transmitted but not detected in the donor), which can lead to underestimated
367 transmission bottlenecks (28). Our formulation of this model incorporates empirically determined
368 sensitivity and specificity metrics to account for both false negative iSNV and false positive iSNV
369 (34). Furthermore, if rare, undetected, iSNV were shared between linked individuals, we would
370 expect to see transmission of more common iSNV (frequency 5-10%), which we can detect with
371 high sensitivity. In our dataset, however, the majority of minority iSNV above 5% were not
372 shared.
373
374 Although the size of our transmission bottleneck is consistent with estimates obtained for other
375 viruses and in experimental animal models of influenza (23, 25), it differs substantially from the
376 only other study of natural human infection (11, 28). While there are significant differences in the
377 design and demographics of the cohorts, the influenza seasons under study, and sequencing
378 methodology, the bottleneck size estimates are fundamentally driven by the amount of viral
379 diversity shared among individuals in a household. Importantly, we used both epidemiologic
380 linkage and the genetic relatedness of viruses in households to define transmission pairs and to
381 exclude confounding from the observed background diversity in the community. Whereas we
382 find that household transmission pairs and randomly assigned community pairs had distinct
383 patterns of shared consensus and minority variant diversity, Poon et al. found that rare iSNV
384 were often shared in both household pairs and randomly assigned community pairs (11).
385
386 Accurately modeling and predicting influenza virus evolution requires a thorough understanding
387 of the virus' population structure. Some models have assumed a large intrahost population and
388 a relatively loose transmission bottleneck (24, 50, 51). Here, adaptive iSNV can rapidly rise in
389 frequency and low frequency variants can have a high probability of transmission. In such a

model, it would be possible for the highly pathogenic H5N1 virus to develop the requisite 4-5 mutations to become transmissible through aerosols during a single acute infection of a human host (50, 52). Although the dynamics of emergent avian influenza and human adapted seasonal viruses likely differ, our work suggests that fixation of multiple mutations over the course of a single acute infection is unlikely.

While it seems counterintuitive that influenza evolution is dominated by drift on local scales and positive selection on global scales, these models are not necessarily in conflict. Within individuals we have shown that the effective population is quite small, which suggests that selection is inefficient. Indeed, we have deeply sequenced 332 intrahost populations from 283 individuals collected over more than 11,000 person-seasons of observation and only identified a handful of minority antigenic variants with little evidence for positive selection (this work and (14)). However, with several million infected individuals each year, even inefficient processes and rare events are likely to happen at a reasonable frequency on a global scale.

Methods

Description of the cohort

The HIVE cohort (30, 31), established at the UM School of Public Health in 2010, enrolled and followed households of at least 3 individuals with at least two children <18 years of age; households were then followed prospectively throughout the year for ascertainment of acute respiratory illnesses. Study participants were queried weekly about the onset of illnesses meeting our standard case definition (two or more of: cough, fever/feverishness, nasal congestion, sore throat, body aches, chills, headache if ≥3 yrs old; cough, fever/feverishness, nasal congestion/runny nose, trouble breathing, fussiness/irritability, decreased appetite, fatigue in <3 yrs old), and the symptomatic participants then attended a study visit at the research clinic

on site at UM School of Public Health for sample collection. For the 2010-2011 through 2013-2014 seasons, a combined nasal and throat swab (or nasal swab only in children < 3 years of age) was collected at the onsite research clinic by the study team. Beginning with the 2014-2015 seasons, respiratory samples were collected at two time points in each participant meeting the case definition; the first collection was a self- or parent-collected nasal swab collected at illness onset. Subsequently, a combined nasal and throat swab (or nasal swab only in children < 3 years of age) was collected at the onsite research clinic by the study team. Families with very young children (< 3 years of age) were followed using home visits by a trained medical assistant.

Active illness surveillance and sample collection for cases were conducted October through May and fully captured the influenza season in Southeast Michigan in each of the study years. Data on participant, family and household characteristics, and on high-risk conditions were additionally collected by annual interview and review of each participant's electronic medical record. In the current cohort, serum specimens were also collected twice yearly during fall (November-December) and spring (May-June) for serologic testing for antibodies against influenza.

This study was approved by the Institutional Review Board of the University of Michigan Medical School, and all human subjects provided informed consent.

Identification of influenza virus

Respiratory specimens were processed daily to determine laboratory-confirmed influenza infection. Viral RNA was extracted (Qiagen QIAamp Viral RNA Mini Kit) and tested by RT-PCR for universal detection of influenza A and B. Samples with positive results by the universal assay were then subtyped to determine A(H3N2), A(H1N1), A(pH1N1) subtypes and B(Yamagata) and B(Victoria) lineages. We used primers, probes and amplification parameters

442 developed by the Centers for Disease Control and Prevention Influenza Division for use on the
443 ABI 7500 Fast Real-Time PCR System platform. An RNAseP detection step was run for each
444 specimen to confirm specimen quality and successful RNA extraction.
445
446 *Quantification of viral load*
447 Quantitative reverse transcription polymerase chain reaction (RT-qPCR) was performed on 5µl
448 RNA from each sample using CDC RT-PCR primers InfA Forward, InfA Reverse, and InfA
449 probe, which bind to a portion of the influenza M gene (CDC protocol, 28 April 2009). Each
450 reaction contained 5.4µl nuclease-free water, 0.5µl each primer/probe, 0.5µl SuperScript III
451 RT/Platinum Taq mix (Invitrogen 111732) 12.5µl PCR Master Mix, 0.1µl ROX, 5µl RNA. The
452 PCR master mix was thawed and stored at 4°C, 24 hours before reaction set-up. A standard
453 curve relating copy number to Ct value was generated based on 10-fold dilutions of a control
454 plasmid run in duplicate.
455
456 *Illumina library preparation and sequencing*
457 We amplified cDNA corresponding to all 8 genomic segments from 5µl of viral RNA using the
458 SuperScript III One-Step RT-PCR Platinum Taq HiFi Kit (Invitrogen 12574). Reactions consisted
459 of 0.5µl Superscript III Platinum Taq Mix, 12.5µl 2x reaction buffer, 6µl DEPC water, and 0.2µl
460 of 10µM Uni12/Inf1, 0.3µl of 10µM Uni12/Inf3, and 0.5µl of 10µM Uni13/Inf1 universal influenza
461 A primers (53). The thermocycler protocol was: 42˚C for 60 min then 94˚C for 2 min then 5
462 cycles of 94˚C for 30 sec, 44˚C for 30 sec, 68˚C for 3 min, then 28 cycles of 94˚C for 30 sec,
463 57˚C for 30 sec, 68˚C for 3 min. Amplification of all 8 segments was confirmed by gel
464 electrophoresis, and 750ng of each cDNA mixture were sheared to an average size of 300 to
465 400bp using a Covaris S220 focused ultrasonicator. Sequencing libraries were prepared using
466 the NEBNext Ultra DNA library prep kit (NEB E7370L), Agencourt AMPure XP beads (Beckman
467 Coulter A63881), and NEBNext multiplex oligonucleotides for Illumina (NEB E7600S). The final

concentration of each barcoded library was determined by Quanti PicoGreen dsDNA quantification (ThermoFisher Scientific), and equal nanomolar concentrations were pooled. Residual primer dimers were removed by gel isolation of a 300-500bp band, which was purified using a GeneJet Gel Extraction Kit (ThermoFisher Scientific). Purified library pools were sequenced on an Illumina HiSeq 2500 with 2x125 nucleotide paired end reads. All raw sequence data have been deposited at the NCBI sequence read archive (BioProject submission ID: SUB2951236). PCR amplicons derived from an equimolar mixture of eight clonal plasmids, each containing a genomic segment of the circulating strain were processed in similar fashion and sequenced on the same HiSeq flow cell as the appropriate patient derived samples. These clonally derived samples served as internal controls to improve the accuracy of variant identification and control for batch effects that confound sequencing experiments.

Identification of iSNV

Intrahost single nucleotide variants were identified in samples that had greater than 10^3 genomes/µl and an average coverage >1000x across the genome. Variants were identified using DeepSNV and scripts available at https://github.com/lauringlab/variant_pipeline as described previously (34) with a few minor and necessary modifications. Briefly, reads were aligned to the reference sequence (H3N2 2010-2011 & 2011-2012 : GenBank CY121496-503, H3N2 2012-2013:GenBank KJ942680-8, H3N2 2014-2015 : Genbank CY207731-8, H1N1 GenBank : CY121680-8) using Bowtie2 (54). Duplicate reads were then marked and removed using Picard (http://broadinstitute.github.io/picard/). We identified putative iSNV using DeepSNV. Bases with phred <30 were masked. Minority iSNV (frequency <50%) were then filtered for quality using our empirically determined quality thresholds (p-value <0.01 DeepSNV, average mapping quality >30, average Phred >35, average read position between 31 and 94). To control for PCR errors in samples with lower input titers, all isolates with titers between 10^3 and 10^5 genomes/µl were processed and sequenced in duplicate. Only iSNV that were found in both

494 replicates were included in down stream analysis. The frequency of the variant in the replicate
495 with higher coverage at the iSNV location was assigned as the frequency of the iSNV. Finally,
496 any SNV with a frequency below 2% was discarded.
497
498 Given the diversity of the circulating strain in a given season, there were a number of cases in
499 which isolates contained mutations that were essentially fixed (>95%) relative to the plasmid
500 control. Often in these cases, the minor allele in the sample matched the major allele in the
501 plasmid control. We were, therefore, unable to use DeepSNV in estimating the base specific
502 error rate at this site for these minor alleles and required an alternative means of eliminating
503 true and false minority iSNV. To this end we applied stringent quality thresholds to these
504 putative iSNV and implemented a 2% frequency threshold. In order to ensure we were not
505 introducing a large number of false positive iSNV into our analysis, we performed the following
506 experiment. Perth (H3N2) samples were sequenced on the same flow cell as both the Perth and
507 Victoria (H3N2) plasmid controls. Minority iSNV were identified using both plasmid controls. This
508 allowed us to identify rare iSNV at positions in which the plasmid controls differed both with and
509 without the error rates provided by DeepSNV. We found that at a frequency threshold of 2% the
510 methods were nearly identical (NPV of 1, and PPV of 0.94 compared to DeepSNV).
511
512 *Overview of models for effective population size*
513 We estimated the effective population size using two separate interpretations of a Wright-Fisher
514 population. At its base, the Wright-Fisher model describes the expected changes in allele
515 frequency of an ideal population, which is characterized by non-overlapping generations, no
516 migration, no novel mutation, and no population structure. We then asked what size effective
517 population would make the changes in frequency observed in our dataset most likely. We
518 calculated these values using two applications of the Wright-Fisher model (i) a diffusion

519 approximation (43) and (ii) a maximum likelihood approach based on the discrete interpretation
520 (44).
521
522 For these estimates we restricted our analysis to longitudinal samples from a single individual
523 that were separated by at least 1 day and only used sites that were polymorphic in the initial
524 sample (29 of the 49 total serial sample pairs). We modeled only the iSNV that were the minor
525 allele at the first time point, and we assumed a within host generation time of either 6 or 12
526 hours as proposed by Geoghegan *et. al* (24).
527
528 *Diffusion approximation*
529 The diffusion approximation was first solved by Kimura in 1955 (43). This approximation to the
530 discrete Wright-Fisher model has enjoyed widespread use in population genetics as it allows
531 one to treat the random time dependent probability distribution of final allele frequencies as a
532 continuous function (e.g. (55-60)). Here, we also included the limitations in our sensitivity to
533 detect rare iSNV by integrating over regions of this probability density that were either below our
534 limit of detection or within ranges where we expect less than perfect sensitivity. Our adaptation
535 of Kimura's original work is below.
536
537 Let $P(p_0, p_t, t \mid N_e)$ be the time dependent probability of a variant drifting from an initial
538 frequency of p_0 to p_t over the course of t generations given an effective population size of N_e
539 where $0 < p_t < 1$.
540
541 The time dependent derivative of this probability has been defined using the forward
542 Kolmogorov equation and the solution is here adapted from Kimura, 1955 (43).
543

$$P(p_0, p_t, t \mid N_e) = \sum_{i=1}^{\infty} p_0\, q_0 i(i+1)(2i+1) F(1-i, i+2, 2, p) \times F(1-i, i+2, 2, p_t) e^{-\left[\frac{i(i+1)}{2N_e}\right]t} \quad (1)$$

Where $q = 1 - p$ and F is the hypergeometric function. We approximated the infinite sum by summing over the first 50 terms. When we added an additional 50 terms (100 in total) we found no appreciable change in the final log likelihoods.

We denote the event that an allele is not observed at the second time point as $p_t \approx 0$ and the probability of such an event as $P(p_0, p_t \approx 0, t \mid N_e)$. This probability is given in equation 2 as the sum of the probability that the variant is lost by generation t (i.e. the other allele is fixed $P(q_0, 1, t \mid N_e)$), the probability that it is not detected due to the limit of detection (i.e. $P(p, p_t \approx 0, t \mid 0 < p_t < 0.02, N_e)$) and the probability the variant is not detected due to low sensitivity for rare variant detection (i.e. $P(p_0, p_t \approx 0, t \mid 0.02 < p_t < 0.1, N_e)$). The probability of not observing an allele at the second time is then

$$P(p_0, p_t \approx 0, t \mid N_e) = P(q_0, 1, t \mid N_e) + P(p, p_t \approx 0, t \mid 0 < p_t < 0.02, N_e) + P(p_0, p_t \approx 0, t \mid 0.02 < p_t < 0.1, N_e) \quad (2)$$

The first term in equation 2 is adapted from Kimura, 1955 as

$$P(q_0, 1, t \mid N_e) = q_0 + \sum_{i=1}^{\infty} (2i+1) p_0 q_0 (-1)^i F(1-i, i+2, 2, q_0) e^{-[i(i+1)/2N_e]t} \quad (3)$$

Where q is defined as above. (Note that this is simply the probability of fixation for a variant at initial frequency q). As in equation 1 the infinite sum was approximated with a partial sum of 50 terms.

The probability of the allele drifting below our limit of detection can be found by integrating equation 1 between 0 and our limit of detection, 0.02. This was done numerically using the python package scipy (61).

$$P(p, p_t \approx 0, t \mid 0 < p_t < 0.02, N_e) = \int_0^{0.02} P\,(p_0, p_t, t|N_e)dp_t \quad (4)$$

Finally, the probability of an iSNV being present at the second time point, but escaping detection, is given by the integral of equation 1 between our benchmarked frequencies (0.02,0.05) times the false negative rate for that range. Here, we assumed the entire range had the same sensitivity as the benchmarked frequency at the lower bound and rounded recipient titers down to the nearest $\log_{10}$ titer (e.g. 10^3,10^4, 10^5). We also assumed perfect sensitivity above 10%.

$$P(p_0, p_t \approx 0, t \mid 0.02 < p_t < 0.1, N_e)) = \sum_{f_i}^{[0.02,0.05,0.10)} (\mathrm{FNR} \mid \mathrm{Titer}_r, f_i) \int_{f_i}^{f_{i+1}} P\,(p_0, p_t, t \mid N_e)dp_t \quad (5)$$

Where $(\mathrm{FNR} \mid \mathrm{Titer}_r, f_i)$ is the false negative rate given the frequency and the sample titer (See Supplemental Table 1) and $P(p_0, p_t, t \mid N_e)$ is defined in equation 1.

The log likelihood of a given population size is then simply the sum of the log of $P(p_0, p_t, t \mid N_e)$ for each minor allele in the data set, where either the position is polymorphic at time t (i.e. equation 1) or the allele is observed as lost at time t (i.e. equation 2)

Discrete Wright-Fisher estimation of N_e

The diffusion approximation treats changes in frequency as a continuous process because it assumes sufficiently large N_e. That assumption can be relaxed, and the effective population size can be determined, by applying a maximum likelihood method developed by Williamsom and Slaktin 1999 (44). In this model, the true allele frequencies move between discrete states (i.e. the frequency must be of the form i/N_e where i is a whole number in the range $[0, N_e]$. In the original application, allele counts were used, and sampling error was added to the model as a binomial distribution with n determined by the sample size. Here, we use the frequencies available from next generation sequencing and estimate sampling error as a normal distribution with mean equal to the observed frequency and a standard deviation equal to that observed in our benchmarking study for the 10^4 genomes/μl samples ($\sigma = 0.014$) (34).

In this model, the probability of observing an allele frequency shift from p_0 to p_t in t generations provided an effective population of N_e is the probability of observing p_0 given some initial state q_0 and the probability of the population having that state, times the probability of observing p_t given some final state q_t and the probability of moving from the initial to the final state summed across all possible states.

$$P(p_0, p_t \mid N_e) = \sum^{q_0, q_t} P(p_0 \mid q_0) P(q_0 \mid N_e) P(p_t \mid q_t) P(q_t \mid q_0, N_e) \quad (6)$$

Where p are the observed probabilities and q are the real ones (of the form i/N_e discussed above). The likelihood of observing a given frequency p_x given a defined state q_x is given by the likelihood of drawing p_x from a normal distribution with mean q_x and standard deviation 0.014.

$$P(p_x \mid q_x) = \mathrm{Norm}(q_x, 0.014) \tag{7}$$

As in Williamson and Slatkin 1999, we assume a uniform prior on the initial state. Because we know that our specificity is near perfect (Supplemental Table 1) and we restrict our analysis to only polymorphic sites, the probability of any initial state is given by

$$P(q_0 \mid N_e) = \frac{1}{N_e - 1} \tag{8}$$

and finally the probability of moving from one state to another in t generations is given by

$$P(q_t, q_0 \mid N_e) = v_0 M^t v_t \tag{9}$$

Where M is a square transmission matrix with $C = N_e + 1$ rows and columns. Where $m_{i,j}$ is the probability of going from the ith configuration to the jth or the probability of drawing $j - 1$ out of binomial distribution with mean $(i - 1)/N_e$ and a sample size N_e. v_0 is a row vector of initial frequencies q_0 with 100% chance of initial state q_0, and v_t is column vector of the frequencies at time point t with 100% chance of the final state. In other words v_0 is a row vector of C states with 0 everywhere except in the ith position where $\frac{i-1}{N_e} = q_0$, and v_t is a column vector of C states with 0 everywhere except the jth position where $\frac{j-1}{N_e} = q_t$

Using the scalar and cumulative properties of matrix multiplication equation 6 reduces to

$$P(p_0, p_t \mid N_e) = [0, P(p_0 \mid q_{0_2})P(q_{0_2} \mid N_e), \ldots, P(p_0 \mid q_{0_{N_e-1}})P(q_{0_{N_e-1}} \mid N_e), 0]M^t \begin{bmatrix} P(p_t \mid q_{t_1}) \\ \vdots \\ P(p_t \mid q_{t_{N_e}}) \end{bmatrix} \tag{10}$$

The first and last entries in v_0 are 0 because we assume all measured sites represent polymorphisms at the first time of sampling. As above, the log likelihood of a given population size is then simply the sum of the log of $P(p_0, p_t, t \mid N_e)$ for each minor allele in the data set.

Simulations

To simulate within host evolution we set N_e in equation 10 to either 30, 50 or 100. For each minor allele we used the closest available non-zero state given the effective population size as the starting state. We then calculated the probability of moving to any other state and selected a final state from this distribution. We then drew a final measured frequency from the normal distribution accounting for measurement errors.

ABC model

We estimated both the effective population size and selection coefficients using the approximate Bayesian computation (ABC) described in (17, 45) with the scripts provided in (45). In its current implementation, this analysis requires the same time points for each sample, and we restricted this analysis to longitudinal samples taken 1 day apart. This subset constitutes 16 of the 29 modeled longitudinal samples. Briefly, we subsampled polymorphic sites to 1,000x coverage to estimate allele counts from frequency data as in (17). We then estimated the prior distribution of the effective population size using 10,000 bootstrap replicates. We selected a uniform distribution on the range [-0.5,0.5] as the prior distribution for the selection coefficients. The posterior distributions were determined from accepting the top 0.01% of 100,000 simulations.

Overview of models used for estimating the transmission bottleneck

We model transmission as a simple binomial sampling process (28). In our first model, we assume any transmitted iSNV, no matter the frequency, will be detected in the recipient. In the second, we relax this assumption and account for false negative iSNV in the recipient. To

include the variance in the transmission bottlenecks between pairs we use maximum likelihood optimization to fit the average bottleneck size assuming the distribution follows a zero-truncated Poisson distribution.

Presence/Absence model

The presence/absence model makes many simplifying assumptions. We assume perfect detection of all transmitted iSNV in the recipient. For each donor iSNV, we measure only whether or not the variant is present in the recipient. Any iSNV that is not found in the recipient is assumed to have not been transmitted. We also assume the probability of transmission is determined only by the frequency of the iSNV in the donor at the time of sampling (regardless of how much time passes between sampling and transmission). The probability of transmission is simply the probability that the iSNV is included at least once in a sample size equal to the bottleneck. Finally, we assume all genomic sites are independent of one another. For this reason, we discarded the one case where the donor was likely infected by two strains as the iSNV were certainly linked.

In our within host models, we only tracked minor alleles as in our data set we only ever find 2 alleles at each polymorphic site. In this case, the frequency of the major allele is simply one minus the frequency of the minor allele. Because the presence/absence model is unaware of the frequency of alleles in the recipient we must track both alleles at each donor polymorphic site.

Let A_1 and A_2 be alleles in some donor j at some genomic site i. Let $P(A_x)$ be the probability that the x allele is the only transmitted allele. There are then three possible outcomes for each site. Either only A_1 is transmitted, only A_2 is transmitted, or both A_1 and A_2 are transmitted. The probability of only one allele being transmitted given a bottleneck size of N_b is

682

$$P_{i,j}(A_x \mid N_b) = p_x^{N_b} \tag{11}$$

683

684 where p_x is the frequency of the x allele in the donor. In other words, this is simply the

685 probability of only drawing A_x in N_b draws.

686

687 The probability of both alleles being transmitted is given by

688

$$P_{i,j}(A_1, A_2 \mid N_b) = 1 - (p_1^{N_b} + p_2^{N_b}) \tag{12}$$

689

690 where p_1 and p_2 are the frequencies of the alleles respectively. This is simply the probability of

691 not picking only A_1 or only A_2 in N_b draws.

692

693 This system could easily be extended to cases where there are more than 2 alleles present at a

694 site; however, that never occurs in our data set.

695

696 For ease we will denote the likelihood of observing the data at a polymorphic site i in each

697 donor j given the bottleneck size N_b as $P_{i,j}(N_b)$ where $P_{i,j}(N_b) = P_{i,j}(A_x \mid N_b)$ if only one allele is

698 transmitted and $P_{i,j}(N_b = P_{i,j}(A_1, A_2 \mid N_b)$ if two alleles are transmitted.

699

700 The log likelihood of a bottleneck of size N_b is given by

701

$$LL(N_b) = \sum_j \sum_i \mathrm{Ln}\,(P_{i,j}) \tag{13}$$

702

703

where Ln is the natural log, and i, j refers to the ith polymorphic site in the jth donor. This is the log of the probability of observing the data summed over all polymorphic sites across all donors. Because the bottleneck size is likely to vary between individuals, we used maximum likelihood to fit the bottleneck distribution as oppose to fitting a single bottleneck value. Under this model we assumed the bottlenecks were distributed according to a zero-truncated Poisson distribution parameterized by λ. The likelihood of observing the data given a polymorphic site i in donor j and λ is

$$P_{i,j}(\lambda) = \sum_{N_b=1}^{\infty} P_{i,j}(N_b) P(N_b \mid \lambda) \quad (14)$$

where $P_{i,j}(N_b)$ is defined as above, $P(N_b \mid \lambda)$ is the probability of drawing a bottleneck of size N_b from a zero-truncated Poisson distribution with a mean of $\frac{\lambda}{1-e^{-\lambda}}$. The sum is across all possible N_b defined on $[1, \infty]$. For practical purposes, we only investigated bottleneck sizes up to 100, as λ is quite small and the probability of drawing a bottleneck size of 100 from a zero-truncated Poisson distribution with $\lambda = 10$ is negligible. We follow this convention whenever this sum appears.

The log likelihood of λ for the data set is given by

$$LL(\lambda) = \sum_{j} \sum_{i} \mathrm{Ln}\left(\sum_{N_b=1}^{\infty} P_{i,j}(N_b) P(N_b \mid \lambda) \right) \quad (15)$$

Beta Binomial model

The Beta binomial model is explained in detail in Leonard *et al.* (28). It is similar to the presence/absence model in that transmission is modeled as a simple sampling process; however, it loosens a few restricting assumptions. In this model, the frequencies of transmitted variants are allowed to change between transmission and sampling according a beta distribution. The distribution is not dependent on the amount of time that passes between transmission and sampling, but rather depends on the size of the founding population (here assumed to equal to N_b) and the number of variant genomes present in founding population k. Note the frequency in the donor is assumed to be the same between sampling and transmission.

The equations below are very similar to those presented by Leonard *et al.* with two exceptions. First, we fit a distribution to the bottleneck sizes in our cohort instead of fitting a single value, and second because we know the sensitivity of our method to detect rare variants based on the expected frequency and the titer, we can include the possibility that iSNV are transmitted but are missed due to poor sensitivity. Because the beta binomial model is aware of the frequency of the iSNV in the recipient, no information is added by tracking both alleles at a genomic site i. Let p_{i,j_d} represent the frequency of the minor allele frequency at position i in the donor of some transmission pair j. Similarly, let p_{i,j_r} be the frequency of that same allele in the recipient of the jth transmission pair. Then, as in Leonard *et al.*, the likelihood of some bottleneck N_b for the data at site i in pair j where the minor allele is transmitted is given by

$$L(N_b)_{i,j} = \sum_{k=1}^{N_b} \text{p\_beta}\left(p_{i,j_r} \mid k, N_b - k\right) \text{p\_bin}\left(k \mid N_b, p_{i,j_d}\right) \quad (16)$$

Where p_beta is the probability density function for the beta distribution and p_bin is the probability mass function for the binomial distribution.

This is the probability density that the transmitted allele is found in the recipient at a frequency of p_{i,j_r} given that the variant was in k genomes in a founding population of size N_b times the probability k variant genomes would be drawn in a sample size of N_b from the donor where the variant frequency was p_{i,j_d}. This is then summed for all possible k where $1 < k \leq N_b$.

As in equation 14 the likelihood of a zero truncated Poisson with a mean of $\frac{\lambda}{1-e^{-\lambda}}$ given this transmitted variants is then given by

$$L(\lambda)_{i,j}^{\text{transmitted}} = \sum_{N_b=1}^{\infty} L\,(N_b)_{i,j} P(N_b \mid \lambda) \tag{17}$$

This is simply the likelihood of each N_b weighted by the probability of drawing a bottleneck size of N_b from bottleneck distribution.

In this model, there are three possible mechanisms for a donor iSNV to not be detected in the recipient. (i) The variant was not transmitted. (ii) The variant was transmitted but is present below our level of detection (2%). (iii) The variant was transmitted and present above our level of detection but represents a false negative in iSNV identification.

As in Leonard *et al.,* the likelihood of scenarios (i) and (ii) for a given N_b are expressed as

$$L(N_b)_{i,j}^{\text{lost}} = \sum_{k=0}^{N_b} \text{p\_beta\_cdf}(p_{i,j_r} < 0.02 \mid k, N_b - k)\text{p\_bin}(k \mid N_b, p_{i,j_d}) \tag{18}$$

Where p_beta_cdf is the cumulative distribution function for the beta distribution. Note that if $k = 0$ (i.e. the iSNV was not transmitted) then the term reduces to the probability of not drawing the variant in N_b draws.

The likelihood of the variant being transmitted but not detected in the recipient given a bottleneck of N_b is described by

$$L(N_b)_{i,j}^{\text{missed}} = \sum_{k=0}^{N_b} \sum_{f_e}^{[0.02,0.05,0.1)} \text{p\_beta\_cdf}(f_e < p_{i,j_r} < f_{e+1} \mid k, N_b - k) \times \text{p\_bin}(k \mid N_b, p_{i,j_d})(\text{FNR} \mid \text{Titer}_r, f_e) \quad (19)$$

This is the likelihood of the variant existing in the ranges [0.0.2,0.05] or [0.05,0.1] given an initial frequency of k/N_b and a bottleneck size of N_b multiplied by the expected False Negative Rate (FNR) given the titer of the recipient and the lower frequency bound. As in our diffusion model, we assumed perfect sensitivity for detection of iSNV present above 10%, rounded recipient titers down to the nearest $\log_{10}$titer (e.g. 10^3,10^4, 10^5) and assumed the entire range $[f_e, f_{e+1}]$ has the same sensitivity as the lower bound.

The likelihood of λ for iSNV that are not observed in the recipient is then given by summing equations 18 and 19 across all possible N_b.

$$L(\lambda)_{i,j}^{\text{nontransmitted}} = \sum_{N_b=1}^{\infty} (L(N_b)_{i,j}^{\text{lost}} + L(N_b)_{i,j}^{\text{missed}}) P(N_b \mid \lambda) \quad (20)$$

The log likelihood of the total dataset is then determined by summing log of equations 17 and 20 (as applicable) across all polymorphic sites in each donor. (As before here we sum of N_b within the range $[1,100]$.)

Simulation

In order evaluate the fits of the two transmission models, we simulated whether or not each donor iSNV was transmitted or not. This involved converting each model to a presence absence model. In each simulation, we assigned a bottleneck from the bottleneck distribution for each transmission pair. We then determined the probability of only transmitting one allele (A_x where $x \in [1,2]$ as in the presence/absence model above) and the probability of transmitted both alleles (A_1, A_2 above) for each polymorphic site.

For the presence/absence model, the probabilities for each possible outcome are given by equations 11 and 12. For the beta binomial model, the probability of only observing A_x at site i is given by

$$P(A_x \mid N_b) = L(N_b)_{i,j}^{\text{lost}} + L(N_b)_{i,j}^{\text{missed}} \quad (21)$$

where $L(N_b)_{i,j}^{\text{lost}}$ and $L(N_b)_{i,j}^{\text{missed}}$ are defined as in equations 18 and 19 respectively, but with p_{i,j_d} replaced by $1 - p_{i,j_d}$. This is simply the probability of not observing the other allele in the recipient.

Again, the probability of observing both alleles is

$$P(A_1, A_2 \mid N_b) = 1 - (P(A_1) + P(A_2))$$

(22)

where $P(A_1)$ and $P(A_2)$ are defined as in equation 21.

Fitting mutation rate and N_e

The diffusion approximation to the Wright - Fischer model allows us to make predictions on the allele frequency spectrum of a population given a mutation rate and an effective population size. The probability of observing a mutation at frequency p_t given an initial frequency of 0 can be approximated as in (2)

$$P(0, p_t, t, \mid \mu, N_e) = \frac{2\mu N_e}{p_t} e^{-\frac{2N_e p_t}{t}}$$

(23)

Where μ is the mutation rate. In this model mutation increases an allele's frequency from 0 but after that initial jump, drift is responsible for allowing the mutation to reach it's observed frequency. Because the limit of equation 23 approaches infinity as p_t approaches 0 and for ease in numerical integration, we assumed that any variant present at less than 0.1% was essentially at 0%.

We then assumed each infection began as a clonal infection matching the consensus sequence observed at the time of sampling. The likelihood of observing minor alleles at the observed frequency is the given by equation 23.

As in the other within host models, we can account for nonpolymorphic sites by adding the likelihood that no mutation is present $P(0, p_t \approx 0, t \mid p_t < 0.001, \mu, N_e)$, that a mutation is present but below our level of detection $P(0, p_t \approx 0, t \mid p_t < 0.02, \mu, N_e)$, and that a mutation is present but missed due to low sensitivity at low frequencies $P(0, p_t \approx 0, t \mid 0.02 < p_t < 0.1, \mu, N_e)$. In this

model we assumed 13133 mutagenic targets in each sample (the number of coding sites present in the reference strain from 2014-2015).

The probability of not observing a mutation is given by

$$P(0, p_t \approx 0, t, \mid \mu, N_e) = P(0, p_t \approx 0, t \mid p_t < 0.001, \mu, N_e) + P(0, p_t \approx 0, t \mid p_t < 0.02, \mu, N_e) + P(0, p_t \approx 0, t \mid 0.02 < p_t < 0.1, \mu, N_e) \quad (24)$$

Where

$$P(0, p_t \approx 0, t \mid p_t < 0.001, \mu, N_e) = 1 - \int_{0.001}^{1} P(0, p_t, t, \mid \mu, N_e) dp_t \quad (25)$$

and

$$P(0, p_t \approx 0, t \mid p_t < 0.02, \mu, N_e) = \int_{0.001}^{0.02} P(0, p_t, t, \mid \mu, N_e) dp_t \quad (26)$$

and

$$P(0, p_t \approx 0, t \mid 0.02 < p_t < 0.1, \mu, N_e) = \sum_{f_i}^{[0.02, 0.05, 0.10)} (\text{FNR} \mid \text{Titer}_r, f_i) \int_{f}^{f_{i+1}} P(p_0, p_t, t \mid \mu, N_e) dp_t \quad (27)$$

Where we follow the same convention as in equation 5 for determining the false negative rate. The log likelihood of a given μ and N_e pair is then the sum of the log of equations 23 and 24 for all possible sites in the data set.

Annotated computer code for all analyses can be accessed at https://github.com/lauringlab/Host_level_IAV_evolution

Acknowledgments

This work was supported by a Clinician Scientist Development Award from the Doris Duke Charitable Foundation (CSDA 2013105), a University of Michigan Discovery Grant, and R01 AI118886, all to ASL. The HIVE cohort was supported by NIH R01 AI097150 and CDC U01 IP00474 to ASM. JTM was supported by the Michigan Predoctoral Training Program in Genetics (T32GM007544). RJW was supported by K08AI119182. We thank Alexey Kondrashov and Aaron King for helpful discussion.

References

1. Kouyos RD, Althaus CL, Bonhoeffer S (2006) Stochastic or deterministic: what is the effective population size of HIV-1? *Trends in Microbiology* 14(12):507–511.

2. Rouzine IM, Rodrigo A, Coffin JM (2001) Transition between stochastic evolution and deterministic evolution in the presence of selection: general theory and application to virology. *Microbiology and Molecular Biology Reviews* 65(1):151–185.

3. Nelson MI, Holmes EC (2007) The evolution of epidemic influenza. *Nat Rev Genet* 8(3):196–205.

4. Holmes EC (2009) RNA virus genomics: a world of possibilities. *Journal of Clinical Investigation* 119(9):2488–2495.

5. Rambaut A, et al. (2008) The genomic and epidemiological dynamics of human influenza A virus. *Nature* 453(7195):615–619.

6. Nelson MI, et al. (2006) Stochastic Processes Are Key Determinants of Short-Term Evolution in Influenza A Virus. *PLoS Pathog* 2(12):e125.

7. Kao RR, Haydon DT, Lycett SJ, Murcia PR (2014) Supersize me: how whole-genome sequencing and big data are transforming epidemiology. *Trends in Microbiology*:1–10.

8. Rogers MB, et al. (2015) Intrahost dynamics of antiviral resistance in influenza a virus reflect complex patterns of segment linkage, reassortment, and natural selection. *mBio* 6(2):e02464–14.

9. Murcia PR, et al. (2010) Intra- and Interhost Evolutionary Dynamics of Equine Influenza Virus. *J Virol* 84(14):6943–6954.

10. Iqbal M, et al. (2009) Within-host variation of avian influenza viruses. *Philosophical Transactions of the Royal Society B: Biological Sciences* 364(1530):2739–2747.

11. Poon LLM, et al. (2016) Quantifying influenza virus diversity and transmission in humans. *Nat Genet* 48(2):195–200.

12. Ghedin E, et al. (2009) Mixed Infection and the Genesis of Influenza Virus Diversity. *J Virol* 83(17):8832–8841.

13. Dinis JM, et al. (2016) Deep Sequencing Reveals Potential Antigenic Variants at Low Frequencies in Influenza A Virus-Infected Humans. *J Virol* 90(7):3355–3365.

14. Debbink K, et al. (2017) Vaccination has minimal impact on the intrahost diversity of H3N2 influenza viruses. *PLoS Pathog* 13(1):e1006194.

15. Doud MB, Hensley SE, Bloom JD (2017) Complete mapping of viral escape from neutralizing antibodies. *PLoS Pathog* 13(3):e1006271.

16. Archetti I, HORSFALL FL (1950) Persistent antigenic variation of influenza A viruses after incomplete neutralization in ovo with heterologous immune serum. *The Journal of Experimental Medicine* 92(5):441–462.

17. Foll M, et al. (2014) Influenza Virus Drug Resistance: A Time-Sampled Population Genetics Perspective. *PLoS Genet* 10(2):e1004185–17.

18. Gubareva LV, Kaiser L, Matrosovich MN, Soo-Hoo Y, Hayden FG (2001) Selection of Influenza Virus Mutants in Experimentally Infected Volunteers Treated with Oseltamivir. *Journal of Infectious Diseases* 183(4):523–531.

19. Ghedin E, et al. (2010) Deep Sequencing Reveals Mixed Infection with 2009 Pandemic Influenza A (H1N1) Virus Strains and the Emergence of Oseltamivir Resistance. *Journal of Infectious Diseases* 203(2):168–174.

20. Xue KS, et al. (2017) Parallel evolution of influenza across multiple spatiotemporal scales. *eLife* 6:46.

21. Sobel Leonard A, et al. (2016) Deep Sequencing of Influenza A Virus from a Human Challenge Study Reveals a Selective Bottleneck and Only Limited Intrahost Genetic Diversification. *J Virol* 90(24):11247–11258.

22. Alizon S, Luciani F, Regoes RR (2011) Epidemiological and clinical consequences of within-host evolution. *Trends in Microbiology* 19(1):24–32.

23. Zwart MP, Elena SF (2015) Matters of Size: Genetic Bottlenecks in Virus Infection and Their Potential Impact on Evolution. *Annual Review of Virology* 2(1):161–179.

24. Geoghegan JL, Senior AM, Holmes EC (2016) Pathogen population bottlenecks and adaptive landscapes: overcoming the barriers to disease emergence. *Proc Biol Sci* 283(1837):20160727–9.

25. Varble A, et al. (2014) Influenza A Virus Transmission Bottlenecks Are Defined by Infection Route and Recipient Host. *Cell Host Microbe* 16(5):691–700.

26. Wilker PR, et al. (2013) Selection on haemagglutinin imposes a bottleneck during

mammalian transmission of reassortant H5N1 influenza viruses. *Nat Comms* 4:1–11.

27. Hughes J, et al. (2012) Transmission of Equine Influenza Virus during an Outbreak Is Characterized by Frequent Mixed Infections and Loose Transmission Bottlenecks. *PLoS Pathog* 8(12):e1003081.

28. Sobel Leonard A, Weissman DB, Greenbaum B, Ghedin E, Koelle K (2017) Transmission Bottleneck Size Estimation from Pathogen Deep-Sequencing Data, with an Application to Human Influenza A Virus. *J Virol* 91(14):e00171–17.

29. Ohmit SE, et al. (2016) Substantial Influenza Vaccine Effectiveness in Households With Children During the 2013–2014 Influenza Season, When 2009 Pandemic Influenza A(H1N1) Virus Predominated. *Journal of Infectious Diseases* 213(8):1229–1236.

30. Ohmit SE, et al. (2015) Influenza Vaccine Effectiveness in Households With Children During the 2012-2013 Season: Assessments of Prior Vaccination and Serologic Susceptibility. *Journal of Infectious Diseases* 211(10):1519–1528.

31. Monto AS, Malosh RE, Petrie JG, Thompson MG, Ohmit SE (2014) Frequency of acute respiratory illnesses and circulation of respiratory viruses in households with children over 3 surveillance seasons. *J Infect Dis* 210(11):1792–1799.

32. Petrie JG, et al. (2013) Influenza transmission in a cohort of households with children: 2010-2011. *PLoS ONE* 8(9):e75339.

33. Chung JR, et al. (2017) Prior season vaccination and risk of influenza during the 2014-2015 season in the U.S. *J Infect Dis* 216(2):284–285.

34. McCrone JT, Lauring AS (2016) Measurements of intrahost viral diversity are extremely sensitive to systematic errors in variant calling. *J Virol* 90(15):JVI.00667–16–6895.

35. Gerstung M, et al. (2012) Reliable detection of subclonal single-nucleotide variants in tumour cell populations. *Nat Comms* 3:811.

36. Lee M-S, Chen JS-E (2004) Predicting Antigenic Variants of Influenza A/H3N2 Viruses. *Emerg Infect Dis* 10(8):1385–1390.

37. Smith DJ, et al. (2004) Mapping the antigenic and genetic evolution of influenza virus. *Science* 305(5682):371–376.

38. Wiley DC, Wilson IA, Skehel JJ (1981) Structural identification of the antibody-binding sites of Hong Kong influenza haemagglutinin and their involvement in antigenic variation. *Nature*.

39. Koel BF, Burke DF, Bestebroer TM (2013) Substitutions near the receptor binding site determine major antigenic change during influenza virus evolution. …. doi:10.1126/science.1240537.

40. Neher RA, Bedford T (2015) nextflu: real-time tracking of seasonal influenza virus evolution in humans. *Bioinformatics* 31(21):3546–3548.

963 41. Caton AJ, Brownlee GG, Yewdell JW, Gerhard W (1982) The antigenic structure of the
964 influenza virus A/PR/8/34 hemagglutinin (H1 subtype). *Cell* 31(2 Pt 1):417–427.

965 42. Xu R, Ekiert DC, Krause JC, Hai R, Crowe JE (2010) Structural basis of preexisting
966 immunity to the 2009 H1N1 pandemic influenza virus. … 328(5976):354–357.

967 43. Kimura M (1955) Solution of a process of random genetic drift with a continuous model.

968 44. Williamson EG, Slatkin M (1999) Using maximum likelihood to estimate population size
969 from temporal changes in allele frequencies. *Genetics* 152(2):755–761.

970 45. Foll M, Shim H, Jensen JD (2015) WFABC: a Wright-Fisher ABC-based approach for
971 inferring effective population sizes and selection coefficients from time-sampled data. *Mol*
972 *Ecol Resour* 15(1):87–98.

973 46. Petrie JG, et al. (2017) Application of an Individual-Based Transmission Hazard Model for
974 Estimation of Influenza Vaccine Effectiveness in a Household Cohort. *Am J Epidemiol*.
975 doi:10.1093/aje/kwx217.

976 47. Visher E, Whitefield SE, McCrone JT, Fitzsimmons W, Lauring AS (2016) The Mutational
977 Robustness of Influenza A Virus. *PLoS Pathog* 12(8):e1005856.

978 48. Pauly MD, Procario MC, Lauring AS (2017) A novel twelve class fluctuation test reveals
979 higher than expected mutation rates for influenza A viruses. *eLife* 6:686.

980 49. Gubareva LV, Kaiser L, Matrosovich MN, Soo-Hoo Y, Hayden FG (2001) Selection of
981 Influenza Virus Mutants in Experimentally Infected Volunteers Treated with Oseltamivir.
982 *Journal of Infectious Diseases* 183(4):523–531.

983 50. Russell CA, et al. (2012) The Potential for Respiratory Droplet-Transmissible A/H5N1
984 Influenza Virus to Evolve in a Mammalian Host. *Science* 336(6088):1541–1547.

985 51. Peck KM, Chan CHS, Tanaka MM (2015) Connecting within-host dynamics to the rate of
986 viral molecular evolution. *Virus Evol* 1(1). doi:10.1093/ve/vev013.

987 52. Herfst S, et al. (2012) Airborne Transmission of Influenza A/H5N1 Virus Between Ferrets.
988 *Science* 336(6088):1534–1541.

989 53. Zhou B, et al. (2009) Single-reaction genomic amplification accelerates sequencing and
990 vaccine production for classical and Swine origin human influenza a viruses. *J Virol*
991 83(19):10309–10313.

992 54. Langmead B, Salzberg SL (2012) Fast gapped-read alignment with Bowtie 2. *Nat*
993 *Methods* 9(4):357–359.

994 55. Zanini F, Puller V, Brodin J, Albert J, Neher RA (2017) In vivo mutation rates and the
995 landscape of fitness costs of HIV-1. *Virus Evol* 3(1):1–12.

996 56. Myers S, Fefferman C, Patterson N (2008) Can one learn history from the allelic
997 spectrum? *Theoretical Population Biology* 73(3):342–348.

998 57. Nagasawa M, Maruyama T (1979) An application of time reversal of Markov processes to

a problem of population genetics. *Advances in Applied Probability*.

58. Kimura M (1971) Theoretical foundation of population genetics at the molecular level. *Theoretical Population Biology* 2(2):174–208.

59. Kimura M, Ohta T (1969) The Average Number of Generations until Fixation of a Mutant Gene in a Finite Population. *Genetics* 61(3):763–771.

60. Kimura M (1964) Diffusion Models in Population Genetics. *Journal of Applied Probability* 1(2):177.

61. Oliphant TE (2007) Python for Scientific Computing. *Comput Sci Eng* 9(3):10–20.

1009 **Figure Legends**

1010 **Figure 1.** Within host diversity of IAV populations. (A) Boxplots (median, 25th and 75th
1011 percentiles, whiskers extend to most extreme point within median ± 1.5 x IQR) of the number of
1012 viral genomes per microliter transport media stratified by day post symptom onset. Notches
1013 represent the approximate 95% confidence interval of the median. (B) Boxplots (median, 25th
1014 and 75th percentiles, whiskers extend to most extreme point within median ± 1.5 x IQR) of the
1015 number of iSNV in 249 high quality samples stratified by day post symptom onset. (C)
1016 Histogram of within host iSNV frequency in 249 high quality samples. Bin width is 0.05
1017 beginning at 0.02. Mutations are colored nonsynonymous (blue) and synonymous (gold) (D)
1018 Location of all identified iSNV in the influenza A genome. Mutations are colored
1019 nonsynonymous (blue) and synonymous (gold) relative to that sample's consensus sequence.
1020 Triangles signify mutations that were found in more than one individual in a given season.
1021
1022 **Figure 2.** Within host dynamics of IAV. (A) Timing of sample collection for 35 paired longitudinal
1023 samples relative to day of symptom onset. Of the 49 total, 35 pairs had minor iSNV present in
1024 the first sample. (B) The change in frequency over time for minority nonsynonymous (blue) and
1025 synonymous (gold) iSNV identified for the paired samples in (A). (C) The distribution of effective
1026 population sizes estimated from 1,000 simulated populations. Simulations were run on
1027 populations with characteristics similar to the actual patient-derived populations and with the
1028 specified effective population size (x-axis). (D) The effect of iteratively removing iSNV with the
1029 most extreme change in frequency (fraction of iSNV removed, x-axis) on the estimated effective
1030 population size. The point represents the estimate when all iSNV are included (32). (E) The
1031 posterior distributions of selection coefficients estimated for the 35 iSNV present in isolates
1032 sampled one day apart. Distributions are colored according to class relative to the sample
1033 consensus sequence, nonsynonymous (blue) synonymous (gold). Variants for which the 95%

1034 highest posterior density intervals exclude 0.0 are noted in the margin.

1035

1036 **Figure 3.** Between host dynamics of IAV. (A) The distribution of pairwise L1-norm distances for
1037 household (blue) and randomly-assigned community (gold) pairs. The bar heights are
1038 normalized to the height of the highest bar for each given subset (47 for household, 1,590 for
1039 community). The red line represents the 5^{th} percentile of the community distribution. (B) Timing
1040 of symptom onset for 52 epidemiologically linked transmission pairs. Day of symptom onset for
1041 both donor and recipient individuals is indicated by black dots. Dashed lines represent pairs that
1042 were removed due to abnormally high genetic distance between isolates, see (A). (C) The
1043 frequency of donor iSNV in both donor and recipient samples. Frequencies below 2% and
1044 above 98% were set to 0% and 100% respectively. (D) The presence-absence model fit
1045 compared with the observed data. The x-axis represents the frequency of donor iSNV with
1046 transmitted iSNV plotted along the top and nontransmitted iSNV plotted along the bottom. The
1047 black line indicates the probability of transmission for a given iSNV frequency as determined by
1048 logistic regression. Similar fits were calculated for 1,000 simulations with a mean bottleneck size
1049 of 1.66. Fifty percent of simulated outcomes lie in the darkly shaded region and 95% lie in the
1050 lightly shaded regions. (E) The outcome from 1,000 simulated “transmission” events with
1051 randomly assigned recipients. The black line represents the observed data, as in (D) the shaded
1052 regions represent the middle 50% and 95% of simulated outcomes. The results from the
1053 simulated logit models were smoothed by plotting the predicted probability of transmission at
1054 0.02 intervals. (F) The beta-binomial model fit. Similar to (D) except the simulated outcomes are
1055 the based on a beta-binomial model using a mean bottleneck of 1.71.

1056

1057 **Figure 4.** Combined estimates of within host mutation rate and effective population size.
1058 Contour plot shows the log likelihood surface for estimates of the effective population size and
1059 neutral mutation rate. The point represents the peak ($\mu = 4x10^{-6}$, $N_e = 33$, log likelihood = -

3,271). Log likelihoods for each contour are indicated.

Supplemental Figure 1. Sequence coverage for all samples. For each sample, the sliding window mean coverage was calculated using a window size of 200 and a step of 100. The distributions of these means are plotted as box plots (median, 25th and 75th percentiles, whiskers extend to most extreme point within median ± 1.5 x IQR) where the y-axis represents the read depth and the x-axis indicates the position of the window in a concatenated IAV genome.

Supplemental Figure 2. Approximate maximum likelihood trees of the concatenated coding sequences for high quality H1N1 samples. The branches are colored by season; the tip identifiers are colored by household. Arrows with numbers indicate consensus and putative minor haplotypes for samples with greater than 10 iSNV.

Supplemental Figure 3. Approximate maximum likelihood trees of the concatenated coding sequences for high quality H3N2 samples. The branches are colored by season; the tip identifiers are colored by household. Arrows with numbers indicate consensus and putative minor haplotypes for samples with greater than 10 iSNV.

Supplemental Figure 4. The effect of titer and vaccination on the number of iSNV identified. (A) The number of iSNV identified in an isolate (y-axis) plotted against the titer (x-axis, genomes/µl transport media). (B) The number of iSNV identified in each isolate stratified by whether that individual was vaccinated or not. Red bars indicate the median of each distribution.

Supplemental Figure 5. Minority nonsynonymous iSNV in global circulation. The global frequencies of the amino acids that were found as minority variants in sample

1086 isolates (x-axis) plotted overtime (y-axis). Each amino acid trace is labeled according to the H3
1087 number scheme. All samples were isolated in December of 2014 (gray line).
1088
1089 **Supplemental Figure 6.** Reproducibility of iSNV identification for paired samples acquired on
1090 the same day. The x-axis represents iSNV frequencies found in the home-acquired nasal swab.
1091 The y-axis represents iSNV frequencies found the clinic-acquired combined throat and nasal
1092 swab.
1093

1094 **Table 1. Influenza viruses over five seasons in a household cohort**

	2010-2011	2011-2012	2012-2013	2013-2014	2014-2015
Households	328	213	321	232	340
Participants	1441	943	1426	1049	1431
Vaccinated, n (%)[a]	934 (65)	554 (59)	942 (66)	722 (69)	992 (69)
IAV Positive Individuals[b]	86	23	69	48	166
H1N1	26	1	3	47	0
H3N2	58	22	66	1	166
IAV Positive Households[c]					
Two individuals	13	2	9	7	23
Three individuals	5	2	3	3	11
Four individuals	-	-	1	2	4
High Quality NGS Pairs[d]	4	1	2	6	39

1095
1096 [a] Self reported or confirmed receipt of vaccine prior to the specified season.
1097 [b] RT-PCR confirmed infection.
1098 [c] Households in which two individuals were positive within 7 days of each other. In cases of trios and quartets, the
1099 putative chains could have no pair with onset >7 days apart.
1100 [d] Samples with $>10^3$ genome copies per µl of transport medium, adequate amplification of all 8 genomic segments,
1101 and average sequencing coverage $>10^3$ per nucleotide.
1102

Table 2. Within host effective population size of IAV

Model	SNV Used	Generation Time (h)	Effective Population Size (95% CI)
Diffusion approximation	All	6	35 (26-46)
	All	12	17 (13-23)
Discrete model	All	6	32 (28-41)
	Nonsynonymous	6	30 (21-40)
	Synonymous	6	37 (27-54)
	All	12	23 (23-29)
	Nonsynonymous	12	19 (19-21)
	Synonymous	12	27 (22-33)

Supplemental Table 1. Sensitivity and specificity of variant detection

Copy Number[a]	Variant Frequency	Original Pipeline[b] Sensitivity	Original Pipeline[b] Specificity	Current Pipeline[c] Sensitivity	Current Pipeline[c] Specificity
$>10^5$	0.05	1	>0.9999	0.85	1.000
	0.02	0.85	0.9999	0.15	1.000
	0.01	0.95	0.9995	-	-
	0.005	0.35	0.9999	-	-
10^4-10^5	0.05	0.95	0.9999	0.85	1.000
	0.02	0.9	0.9999	0.15	1.000
	0.01	0.8	0.9998	-	-
	0.005	0.4	0.9999	-	-
10^3-10^4	0.05	0.8	>0.9999	0.70	1.000
	0.02	0.45	0.9999	0.15	1.000
	0.01	0.2	0.9997	-	-
	0.005	0.1	0.9999	-	-

[a] Per µl transport media
[b] As described in McCrone JT and Lauring AS, J. Virol. 90(15):6884, 2016.
[c] As described in Methods, benchmarked for frequencies 0.02-0.98 only

Supplemental Table 2. Nonsynonymous substitutions in HA antigenic sites

House ID	Enrolment ID	Symptom Onset	Subtype	Frequency	Amino Acid Change	Antigenic Site	Vaccinated	Day of Symptoms
1111	300481	3-30-2011	H3N2	0.071	E62G	E*	No	0
2166	320661	2-13-2012	H3N2	0.071	V297A	C	Yes	1
1302	301355	3-20-2011	H3N2	0.088	L86I	E	Yes	1
3075	331045	12-10-2012	H3N2	0.066	I214T	D	Yes	1
5219	50935	12-5-2014	H3N2	0.175	F193S	B*†	No	3
5263	51106	12-6-2014	H3N2	0.111	T128A	B	Yes	3
5290	51225	12-15-2014	H3N2	0.405	I260V	E*	Yes	1
5302	51273	12-13-2014	H3N2	0.030	S262N	E*	Yes	0
5098	50419	12-22-2014	H3N2	0.364	G208R	D	Yes	4
5033	50141	12-3-2014	H3N2	0.032	A163T	B	Yes	2
5034	50143	1-11-2015	H3N2	0.119	I307R	C	Yes	1
5289	51220	12-13-2014	H3N2	0.038	K189N	B*†	Yes	-1
5033	50141	12-3-2014	H3N2	0.025	D53E	C*	Yes	1
5033	50141	12-3-2014	H3N2	0.023	S312G	C	Yes	1
5269	51132	12-6-2014	H3N2	0.028	I242T	D	Yes	2
5147	50630	11-18-2014	H3N2	0.164	I242L	D	Yes	1
5034	50143	1-11-2015	H3N2	0.161	I307R	C	Yes	2
4185	UM40738	12-14-2013	H1N1	0.021	R208K	Ca	No	2

* Sites observed to vary between antigenically distinct strains in Wiley et al., 1981 and Smith DJ et al., 2004.
† Sites located in the “antigenic ridge” identified in Koel et al., 2013.

Figure 1

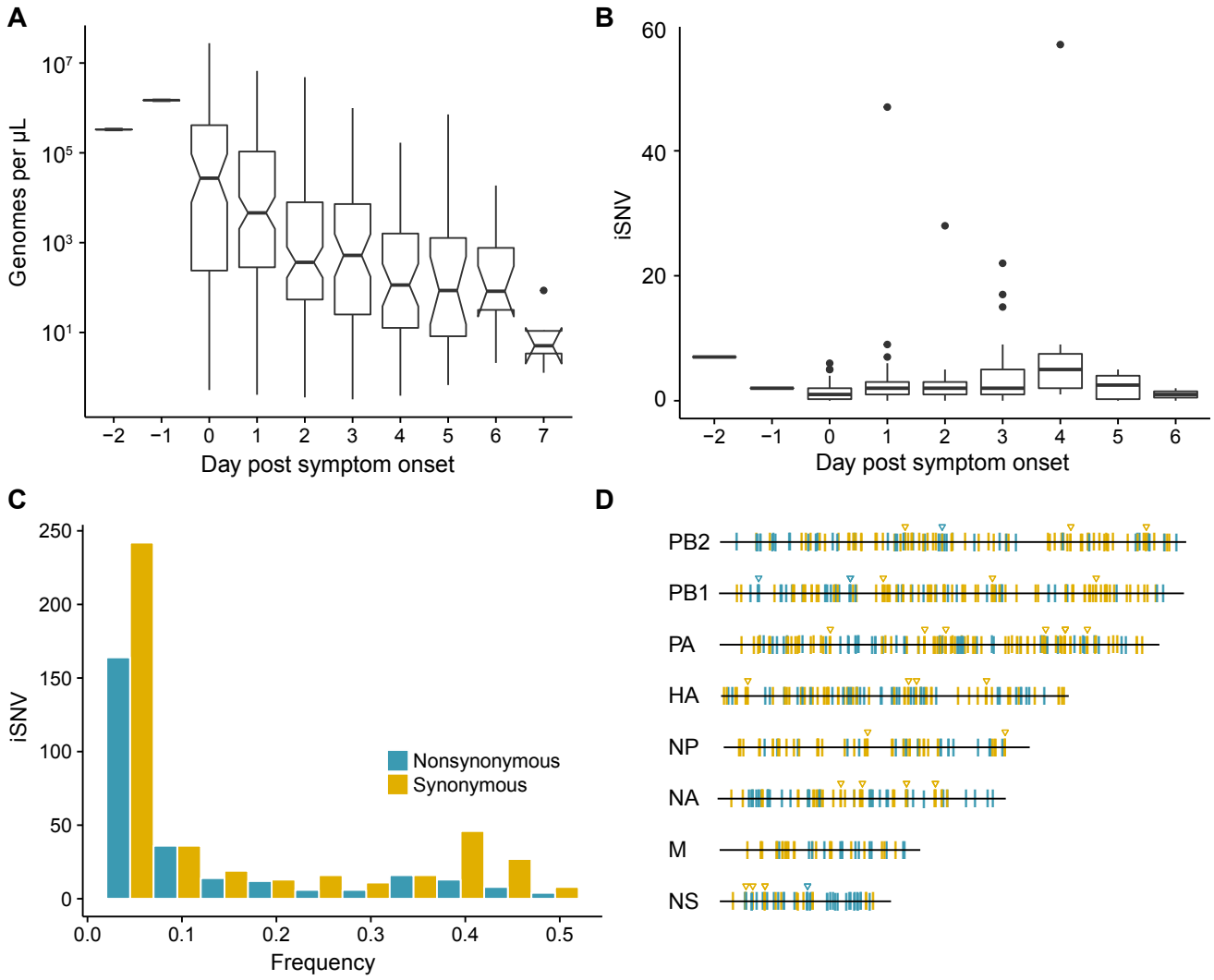

Figure 2

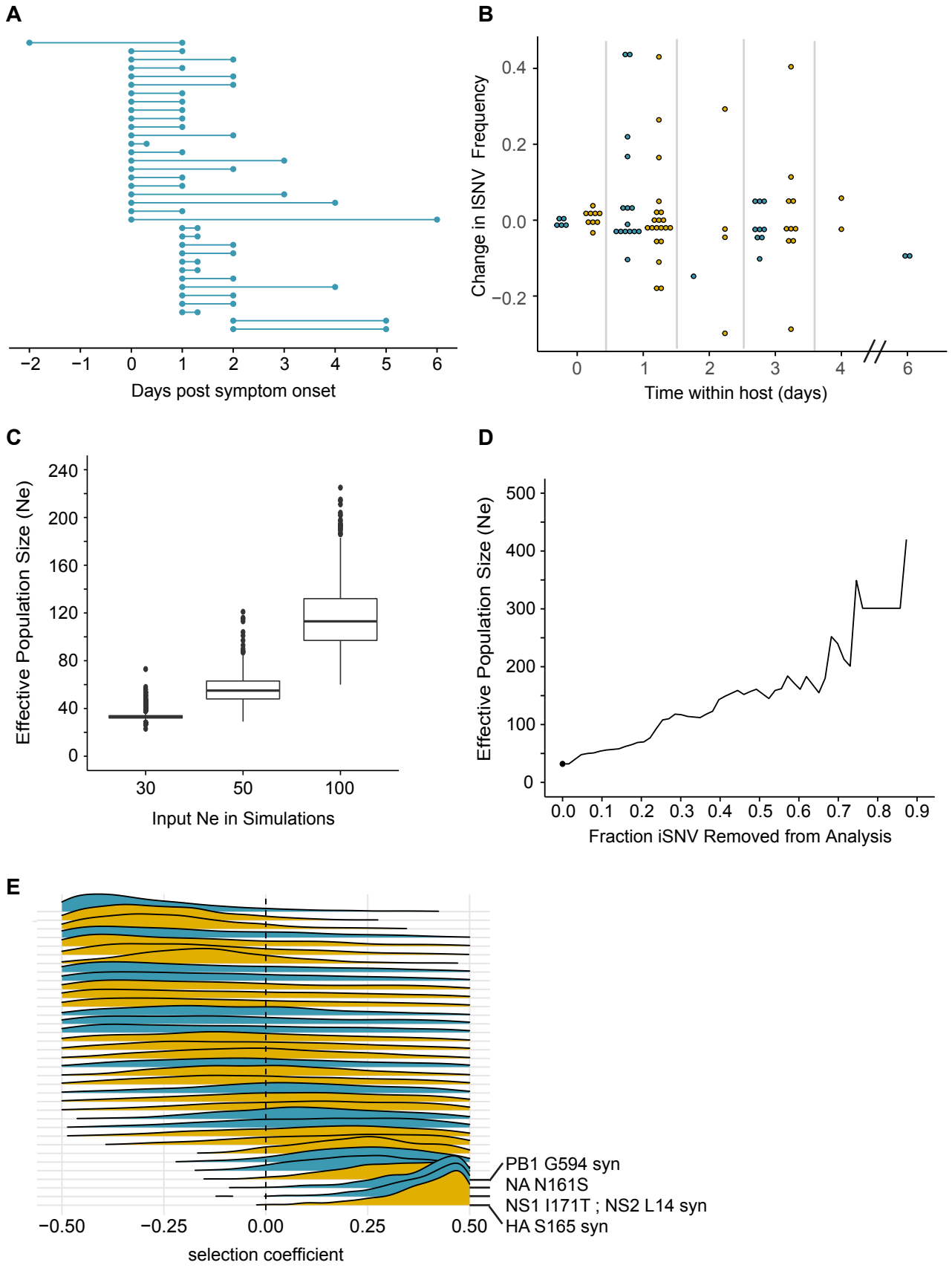

Figure 3

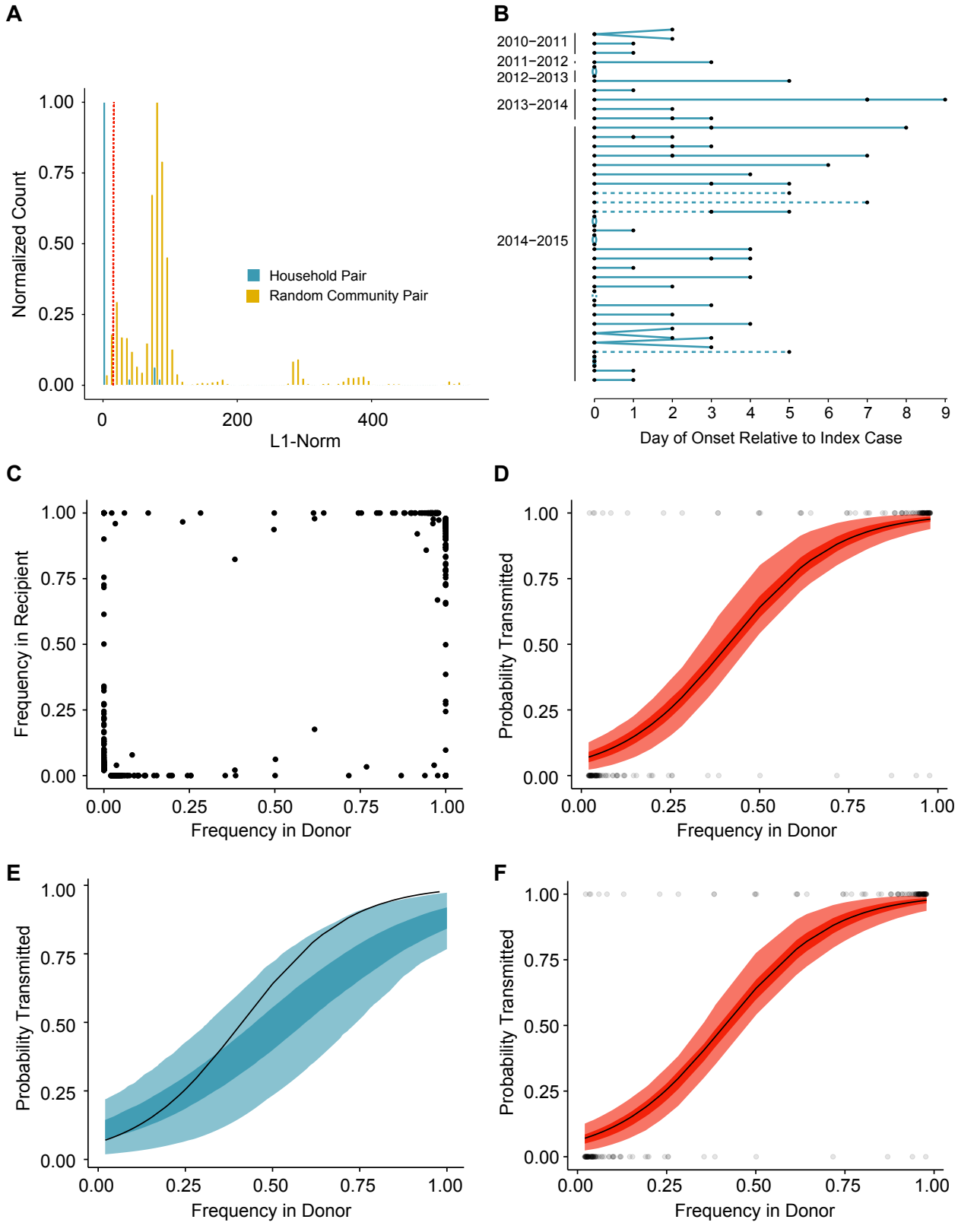

Figure 4